Distributed Microgrid Synchronization Strategy Using a Novel Information Architecture Platform

Yuhua Du, Hao Tu, Srdjan Lukic
FREEDM Systems Center
North Carolina State University
Raleigh, NC, USA
{ydu7, htu, smlukic} @ncsu.edu

Abhishek Dubey, Gabor Karsai
Institute for Software Integrated Systems
Vanderbilt University
Nashiville, TN, USA
{abhishek.dubey, gabor.karsai} @vanderbilt.edu

***Abstract*—To seamlessly reconnect an islanded microgrid to the main grid, voltage phasors on both sides of the point of common coupling need to be synchronized before the main relay closes. In this paper, a distributed control strategy is proposed for microgrid synchronization operation. The proposed controller design utilizes pinning-based consensus algorithm to avoid system single point of failure. It is able to actively track the main grid frequency, provide a good coordination between frequency and phase regulation and ensure all distributed generations in the system proportionally share the load. Implementation of such distributed algorithm in practice is difficult because it requires mitigation of both distributed computing and power system engineering challenges. In this paper, a novel software platform called RIAPS platform is presented that helps implementing the proposed distributed synchronization strategy in practical hardware controllers. The performance of the controllers are validated using a real-time controller hardware-in-the-loop microgrid testbed.**

***Index Terms*—consensus algorithm, distributed control, distributed generation, microgrid synchronization**

I. Introduction

The grid of tomorrow will have to manage variable generations from renewables, which are dispersed across the distribution system. This is leading to increased interest in development of microgrids (MGs) that makes the control of the grid more scalable and resilient. To promote resiliency, such MGs need to operate in both grid connected and islanded mode, and should be able to seamlessly transition between the two modes. For an islanded MG, steady state deviations in system voltage and frequency results from primary control. Secondary control eliminates these deviations and brings the system back to nominal operating states. However, to have the MG reconnect back to the main grid without any inrush transients, the voltage phasors on both sides of the point of common coupling (PCC) need to be synchronized [1].

Most commercial solutions for MG synchronization rely on a single distributed generation (DG) as primary device for regulation [2]. This approach simplifies the requirement of communication and coordination among multiple devices but needs the capacity of the primary DG to be large. It becomes challenging when there are multiple small DGs in the MG, none of which is large enough to dominate the system power flow. Such solution becomes economically unfeasible for larger MGs. Alternate algorithms that allow multiple DGs to coordinate and contribute to eliminate the voltage phasor mismatch exist. However, many of them use a centralized approach, where a MG centralized controller (MCC) is present as a master controller while all the dispatchable DGs act as slave units [3]. Such systems utilize global information exchange, which requires a reliable communication network and brings the risk of single point of failure to the system. Therefore, researchers are favoring the development of distributed control strategies inspired by the concepts of multi-agent systems (MAS) [4]–[6]. In such systems, each DG operates as an intelligent and independent agent that only exchanges information with its neighbors. No delicate communication system is needed and MAS usually run on sparse communication network.

Voltage phasor consists of three elements: voltage magnitude, frequency and phase with respect to a given reference. In an inductive MG, system voltage magnitude is usually decoupled with the other states and could be directly regulated to track the voltage of the main grid [7]. Frequency regulation and phase regulation are challenging as they are naturally coupled: phase could only be regulated with frequency deviation, while a well regulated frequency would result in a constant phase deviation. Some works try to circumvent such conflict by regulating only phase mismatch while ignoring dynamic response of system frequency [8]. However, such approach will result in unbounded system frequency variation which could potentially destabilize the system. Additionally, it has been assumed in most works that the main grid operates constantly as rated and thus the islanded MG is regulated to 60 Hz by default [9]. However, such assumption might not necessarily be the case and the main grid frequency should be actively followed in case of any variation. Explicit regulations on both system frequency and phase are needed to ensure desirable system operation performance. Furthermore, unlike conventional generators, DGs usually have limited power/energy capacities. Besides having all the DGs contribute to the MG synchronization, they should also be able to track and proportionally share the system's total power consumption for system resiliency.

Despite the vast efforts done on developing algorithms for MG synchronization, little has been done on implementing the analytically developed algorithms under hardware level. Each

978-1-4799-7312-5/18/$31.00 ©2018 IEEE

developed algorithms has to repeatedly solve the challenges of distributed computing systems, including information exchange, time synchronization, fault-tolerance, distributed coordination etc, while improving upon the efficacy of the core distributed control concepts. These challenges it difficult to implement these algorithms in practice.

In this paper, we propose a distributed MG synchronization control strategy. The proposed controller design is able to explicitly regulate system frequency, phase and voltage magnitude simultaneously. MG frequency is regulated to the main grid frequency measured in real-time instead of a default value. Additionally, proportional active/reactive power sharing among all the DGs are guaranteed. Stability analysis of the proposed controller design is derived. To have the proposed controller fully implemented under hardware level for further validation, a novel software platform developed by our team, called 'Resilient Information Architecture Platform for Smart Grid' (RIAPS), is introduced. The platform abstracts away the core distributed system problems and enables easy and modular implementation of the control algorithm. The proposed algorithm is then fully realized and validated on a real-time controller hardware-in-the-loop (CHIL) MG testbed.

The rest of this paper is constructed as follows. In Section II, the proposed MG synchronization controller is presented. Stability analysis of the proposed controller is derived and conditions under which the system is exponentially stable are provided. In Section III, RIAPS platform is proposed to address the identified hardware implementation challenges. In Section IV, implementations of the proposed controller using RIAPS platform are discussed in details and validations using a real-time CHIL MG testbed are presented in Section V. Finally conclusions follow in Section VI.

II. Proposed MG Synchronization Control Strategy

As previously reviewed, dispatchable resources within an islanded MG need to actively and accurately regulate their operation states to achieve MG synchronization. Inverter-interfaced DGs have been widely utilized in modern MG and they can be classified as grid-forming DGs or grid-following DGs depending on the characteristic of the resources they are interfacing [10]: dispatchable resources, like generator or energy storage device, are usually interfaced as grid-forming DG and operate as slack bus to stabilize the islanded MG, while intermittent and uncontrollable resources, like PV or wind, are usually interfaced as grid-following DG and inject grid-synchronized current to the external system. In this paper, we consider the DGs under discussion are all grid forming DGs and are equipped with droop controller for inductive system as primary control [11]. Grid following DGs are accounted for in the model as being a part of the stochastic load profile.

Due to the nature of MG synchronization problem, the voltage phasor mismatch on both sides of PCC in frequency, phase and magnitude are usually measured by the main relay and not locally accessible to all the DGs. Pinning-based consensus algorithm is utilized in this paper to avoid additional communication channels. The measured voltage phasor mismatch is only shared to the pinned DG(s) while all the DGs operate coordinately through a sparse communication network. A DG is called phasor regulation DG if it is pinned, otherwise it is called supporting DG.

It is assumed that the MG communication topology is fixed and is modeled by a digraph, $G = (V, \varepsilon, A)$ where $V = \{v_1, v_2, \dots v_n\}$ denotes the set of droop-controlled DGs, $\varepsilon \subseteq V \times V$ denotes valid communication links between DGs and A is the weighted adjacency matrix defined as $a_{ii} = 0$ and $a_{ij} = 1$ if and only if the edge $\{v_i, v_j\} \in \varepsilon$. We denote $\mathbf{L}$ as the Laplacian matrix of G.

A. Frequency/phase regulation controller

The proposed frequency/phase regulation controller is defined as follows:

$$\omega_i = \omega^* - m_i P_i + \Omega_i \tag{1a}$$

$$-\frac{d\Omega_i}{dt} = k_f(\omega_i - \widehat{\omega}_i) + k_P \sum_{j=1}^{N} a_{ij}(\Omega_i - \Omega_j) + r_i \Delta\delta_C \tag{1b}$$

where for the $i-th$ DG ($i = 1, \cdots, N$), ω_i and ω^* present its measured and rated operation frequency; m_i presents the designed droop control gain; P_i presents the measured active power output; $\Delta\delta_C$ presents the measured phase mismatch between the islanded MG and the main grid at PCC; k_f, k_P and r_i present the designed control gains: $r_i = r > 0$ if the $i-th$ DG is selected to be the phasor regulation DG, otherwise $r_i = 0$; Ω_i presents the frequency/phase control variable; $\widehat{\omega}_i$ presents the corrected frequency regulation term that is used to track the main grid frequency and is defined as:

$$\widehat{\omega}_i = \begin{cases} \omega_G & r_i > 0 \\ \omega^* - k_\omega \int \sum_{j=1}^{N} a_{ij}(\widehat{\omega}_i - \widehat{\omega}_j)dt & \text{otherwise} \end{cases} \tag{2}$$

where ω_G presents the measured main grid frequency from the main relay and k_ω presents the designed controller gain. (2) indicates that the measured main grid frequency will be utilized directly by the phasor regulation DG(s) for correction and eventually shared to all the supporting DGs using a standard pinning-based consensus algorithm [12], where the supporting DGs that have direct communication links with the phasor regulation DG(s) are pinned.

In steady state, the frequency correction terms in each DG are uniform and converge to the measured main grid frequency ($\widehat{\omega}_i = \widehat{\omega}_j = \omega_G$, for $i, j = 1, \cdots, N$). The derivation in (1b) becomes zero and the following statements are true: 1) $\omega_i = \widehat{\omega}_i = \omega_G$, meaning that the frequency mismatch between the main grid and islanded MG is eliminated; 2) $\Omega_i = \Omega_j$, meaning that the droop curves in each DG have been shifted equally, indicating proportional active power sharing among DGs [13]; 3) $\Delta\delta_C = 0$, meaning that the phase mismatch between the main grid and islanded MG is eliminated.

B. Voltage regulation controller

As reviewed, voltage regulation is decoupled from frequency/phase regulation and thus can be done separately. The proposed voltage regulation controller is defined as follows:

$$E_i = E^* - n_i Q_i + e_i \tag{3a}$$

$$-\frac{de_i}{dt} = k_Q \sum_{j=1}^{N} a_{ij}\left(\frac{Q_i}{Q_i^*} - \frac{Q_j}{Q_j^*}\right) + \beta_i \Delta E_C \tag{3b}$$

where for the $i-th$ DG, E_i and E^* presents its measured and rated voltage; n_i is the designed droop gain; Q_i and Q_i^* present the measured and rated reactive power output; e_i is the voltage regulation variable; k_Q is the designed regulation gain; β_i is the designed magnitude regulation gain, $\beta_i = \beta > 0$ if the $i-th$ DG is selected to be the phasor regulation DG, otherwise $\beta_i = 0$; ΔE_C presents the voltage magnitude mismatch between the main grid and the islanded MG.

The presented voltage regulation controller is constructed based on the distributed average consensus control proposed in [14] and modified into the form of pinning-based consensus for MG synchronization problem. In steady state, the following statements are true: 1) $\frac{Q_i}{Q_i^*} = \frac{Q_j}{Q_j^*}$, meaning that proportional DG reactive power output is achieved; 2) $\Delta E_C = 0$, meaning that the voltage magnitude mismatch between the main grid and islanded MG is eliminated.

C. Stability analysis

The small-signal stability analysis of the proposed control strategy is derived. System frequency is a global variable and converges fast enough across the system, thus the delay in adjusting DG operation frequency is ignored. We model the delay in adjusting DG output voltage as a first-order low pass filter for simplification. Additionally, considering the fact that frequency variations in the main grid, if any, should still be bounded closely to the rated frequency, it is assumed that the frequency correction term, $\widehat{\omega}_i$ converges fast enough and $\widehat{\omega}_i = \widehat{\omega}_j = \omega_G$ for the subsequent analysis. The operation status of the $i-th$ DG are modeled as:

$$\dot{\delta}_i = -m_i \frac{E_i E_C}{X_i} sin(\delta_i - \delta_C) + \Omega_i \tag{4a}$$

$$\omega_v^{-1} \dot{E}_i = E^* - E_i - n_i \frac{(E_i - E_C)E_C}{X_i} cos(\delta_i - \delta_C) + e_i \tag{4b}$$

where δ_C and δ_i presents the voltage phase at PCC and the $i-th$ DG, respectively; E_C presents the voltage magnitude at PCC; X_i presents the equivalent reactance between the $i-th$ DG and PCC, ω_v presents cut-off frequency of the equivalent low-pass filter.

The system small-signal model is derived by assuming that $sin(\delta_i - \delta_C) \approx \delta_i - \delta_C$ and $E_C = E^*$. Referring to the conditions under which droop control is validated: system active power flow should be predominately determined by phase angle while system reactive power flow should be mainly dependent on bus voltage magnitude [15], it is assumed that $E_i \approx E'$ is constant in (4a) and $cos(\delta_i - \delta_C) \approx 1$ is constant in (4b). Additionally, referring to Millman's Theorem, the voltage phasor at PCC is dependent on the voltage phasors at each DG as $\delta_C = \sum c_i \delta_i$ and $E_C = \sum d_i E_i$ where $c_i = \frac{X_p}{X_i}$ and $d_i = \frac{E_i}{E_C} c_i \approx \frac{E'}{E^*} c_i$ with $X_P^{-1} = \sum X_i^{-1}$ for $i = 1, \cdots, N$. Both c_i and d_i are treated as constants for the subsequent analysis and the small-signal model of the system operation states can be written in matrix form as:

$$\dot{\delta} = -\mathbf{mM}(\mathbf{I} - \mathbf{c})\delta + \mathbf{\Omega} \tag{5a}$$

$$\omega_v^{-1} \dot{\mathbf{E}} = -\mathbf{E} - \mathbf{nN}(\mathbf{I} - \mathbf{d})\mathbf{E} + \mathbf{e} \tag{5b}$$

where δ and $\mathbf{E}$ are system operation states, $\mathbf{mM} = diag(m_i M_i)$ and $\mathbf{nN} = diag(n_i N_i)$ with $M_i = \frac{E' E^*}{X_i}$ and $N_i = \frac{E^*}{X_i}$; $\mathbf{c} = [\mathbf{1}]_\mathbf{N} diag(c_i)$ and $\mathbf{d} = [\mathbf{1}]_\mathbf{N} diag(d_i)$ with $[\mathbf{1}]_\mathbf{N}$ presenting a N-by-N all-ones matrix; $\mathbf{I}$ presents the identical matrix. It is noteworthy that in (5), terms that are independent from system operation states have been ignored.

Assume all the variables are in per unit, the proposed MG synchronization controller can be modeled as:

$$\dot{\mathbf{\Omega}} = k_f \mathbf{mM}(\mathbf{I} - \mathbf{c})\delta - k_f \mathbf{\Omega} - k_P \mathbf{L}\mathbf{\Omega} - \mathbf{rc}\delta \tag{6a}$$

$$\dot{\mathbf{e}} = -k_Q \mathbf{LN}(\mathbf{I} - \mathbf{d})\mathbf{E} - \mathbf{bdE} \tag{6b}$$

where $\mathbf{r} = diag(r_i)$ and $\mathbf{b} = diag(\beta_i)$.

Combining (5) and (6), the small-signal model of the whole system can be written as:

$$\dot{\mathbf{X}} = \mathbf{W}\mathbf{X} \tag{7}$$

where $\mathbf{X}=\begin{pmatrix}\delta & \mathbf{\Omega} & \mathbf{E} & \mathbf{e}\end{pmatrix}'$, $\mathbf{W}=\begin{pmatrix}\mathbf{W_1} & \mathbf{0} \\ \mathbf{0} & \mathbf{W_2}\end{pmatrix}$ presents the system matrix and $\mathbf{W_2}=\begin{pmatrix}\omega_v[-\mathbf{I} - \mathbf{nN}(\mathbf{I} - \mathbf{d})] & \omega_v \mathbf{I} \\ -k_Q \omega_v \mathbf{LN}(\mathbf{I} - \mathbf{D} - \mathbf{bd}) & \mathbf{0}\end{pmatrix}$, $\mathbf{W_1}=\begin{pmatrix}-\mathbf{mM}(\mathbf{I} - \mathbf{c}) & \mathbf{I} \\ (k_f \mathbf{mM}(\mathbf{I} - \mathbf{c}) - \mathbf{rc} & -k_f \mathbf{I} - k_P \mathbf{L}\end{pmatrix}$. Considering the fact that $\mathbf{W}$ is a diagonal matrix, the system is exponentially stable if and only if all the eigenvalues of both $\mathbf{W_1}$ and $\mathbf{W_2}$ have strictly negative real parts.

At last, we derive the sufficient conditions under which the system is exponentially stable. The characteristic polynomial of $\mathbf{W_1}$ can be written as:

$$det(s\mathbf{I} - \mathbf{W_1}) = det(s\mathbf{I} + k_f \mathbf{I} + k_P \mathbf{L}) det(s^2 \mathbf{I} + \mathbf{a_1} s + \mathbf{a_0}) \tag{8}$$

where $\mathbf{a_0} = k_P \mathbf{mM}(\mathbf{I} - \mathbf{c}) + \mathbf{rc}$ and $\mathbf{a_1} = \mathbf{mM}(\mathbf{I} - \mathbf{c}) + k_f \mathbf{I} + k_P \mathbf{L}$. It can be easily observed that the roots of $det(s\mathbf{I} + k_f \mathbf{I} + k_P \mathbf{L})$ satisfy $Re(s) < 0$. For $det(s^2 \mathbf{I} + \mathbf{a_1} s + \mathbf{a_0})$, referring to Routh-Hurwitz stability criterion, it is proved in [13] that roots of such characteristic polynomial satisfies $Re(s) < 0$ if and only if the following conditions are satisfied:

$$\lambda_{min}(\mathbf{a_1} + \mathbf{a_1}^T) > 0 \tag{9a}$$

$$\lambda_{min}(\mathbf{a_0} + \mathbf{a_0}^T) > 0 \tag{9b}$$

We assume that the system is sufficiently similar so that $c_i \approx c_j \approx N^{-1}$, which can be easily achieved by implementing

virtual impedance on each DG. It can be proved that $\mathbf{a_1} + \mathbf{a_1^T}$ is positive definite and condition (9a) is always satisfied. For $\mathbf{a_0}$, we first set $\mathbf{r} = 0$ and it can be proved that $\mathbf{a_0} + \mathbf{a_0^T}$ is positive semi-definite with one zero eigenvalue. Consider the fact that eigenvalues are continuous functions of matrix parameters, condition (9b) can still be satisfied when $r > 0$ is sufficiently small. To conclude, all the roots of $\mathbf{W_1}$ satisfy $Re(s) < 0$ if $c_i \approx c_j$ and $\mathbf{r} > \mathbf{0}$ is sufficiently small.

The same derivation approach can be applied to $\mathbf{W_2}$ and it can be found that all the roots of $\mathbf{W_2}$ satisfy $Re(s) < 0$ if $d_i \approx d_j$ and $\mathbf{b} > \mathbf{0}$ is sufficiently small. It is concluded that sufficient conditions under which the system is exponentially stable are: the system is sufficiently similar ($c_i \approx c_j$ and $d_i \approx d_j$) and the regulation control gains on phase and voltage mismatch ($\mathbf{r} > \mathbf{0}$ and $\mathbf{b} > \mathbf{0}$) are sufficiently small.

III. Hardware Level Implementation Challenges and RIAPS System Overview

The algorithm proposed in the previous section was first implemented and tested using simulation software (i.e. MATLAB/Simulink). Such simulation approach has been adopted by most researchers to simulate and verify their proposed algorithms. However, it has been found that these simulations may be too ideal and oversimplified, suggesting need for Controller Hardware-in-the-loop (CHIL) tests. However, implementation challenges at the hardware level present additional hurdles beyond the traditional control system challenges. We describe some of these challenges below:

- Because of the nature of digital control, the hardware controllers need to have sufficient computational capability, so that the selected sampling time step can be made small enough to minimize the impact caused by transforming from continuous mode to discrete mode.
- The developed distributed control algorithm utilizes multi-agent control approach where the number of participating agents can be large and variable. Therefore, the controller and the hardware implementation must be scalable and should support plug-and-play capability.
- Each agent has to have the capability to interact with physical devices such as PMU. Developing reusable device interaction code that is modular presents additional challenges that are orthogonal to the development of the core control algorithm.
- Though distributed control algorithms do not require delicate communication network compared to centralized ones, reliable and accurate information exchange are still crucial towards system stability because of the small system inertia. Information exchange among distributed hardware controllers requires complement communication system which is also challenging

To overcome the identified challenges, we have developed an framework called RIAPS platform. It is an *open application platform* that distributes the intelligence and control capability to local endpoints reducing total network traffic, improving speed of local actions by avoiding latency, and improving reliability by reducing dependencies on numerous devices and communication interfaces. The platform is multi-tasking and able to host multiple applications running simultaneously. The key concept is to provide a "middleware" that enables each agent to communicate with others and focuses on specific grid issues, such as state estimation, remedial action schemes, and load shedding. More applications developed using RIAPS can be found in [16] and [17].

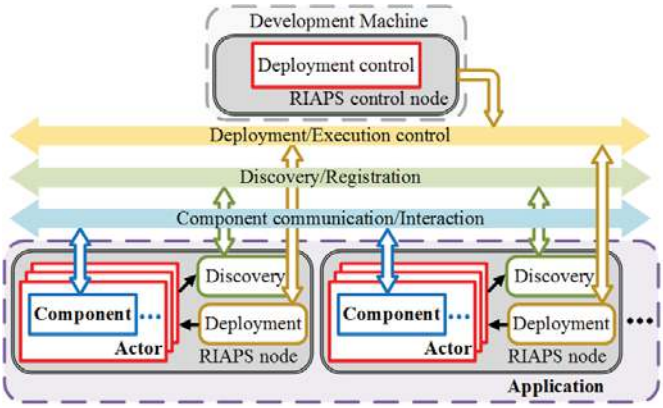

Fig. 1: RIAPS platform architecture overview

An overview of RIAPS platform architecture is presented in Fig. 1. The developed distributed control algorithms in RIAPS platform are called **applications** which reside in the top layer. One **application** consists of one or more application managers, called **actors**. An **actor** is used to realize an abstract function, like state estimation or data logging. Each **actor** is constructed by one or more **components**. The **component** is a reusable building block in RIAPS platform that provides specific physical functionality, like computation or measurement sensing. Each **component** can have several kinds of ports to support its function. For example a timer port which wakes up every time step is usually implemented to achieve discrete calculation. Other ports include publish and subscribe port to publish and subscribe messages, respectively. For a given distributed control algorithm that has been developed analytically, it can be converted into the form of **application** in a development machine. The developed **application** can then be distributed to each RIAPS node through RIAPS deployment mechanism.

Additionally, RIAPS platform provides programming APIs to help development of device wrappers (examples include but not limited to Modbus and IEEE C37.118.2 synchrophasor data transfer protocol) and supports ZeroMQ based messaging paradigm for information exchange between various RIAPS nodes. Message is defined by RIAPS as structured information exchanged between RIAPS nodes. Each subscribe port and publish port are associated with a message with a specific topic. When one publish port publishes a message, the subscribe port that subscribes that message will receive it automatically. This routing of messages is handled by RIAPS discovery service. Available communication patterns include both group-based publish-subscribe as well as point to point client server mechanisms.

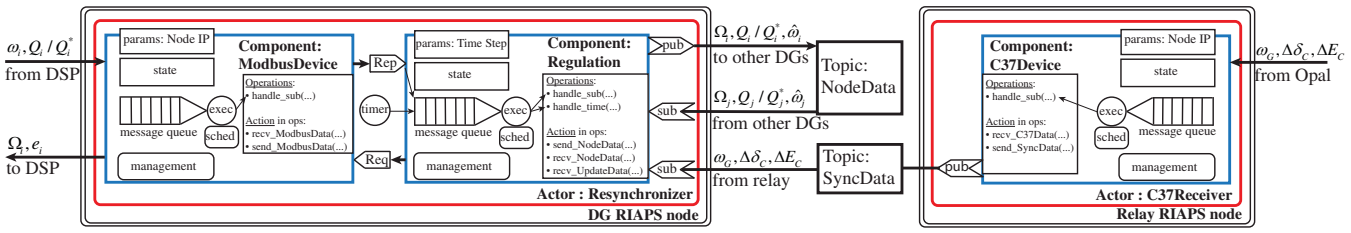

Fig. 2: Architecture of a RIAPS **actor** for phasor regulation DG

IV. Implementation of the Proposed Algorithm in the RIAPS Platform

The proposed MG synchronization algorithm has been fully implemented in the RIAPS platform. Each DG is assigned with one DG RIAPS node. Besides the DG RIAPS nodes, a relay RIAPS node is associated with the main relay at PCC. Fig. 2 shows the architecture of the RIAPS **application** for the propose synchronization algorithm.

The **application** has two actors. The first one is called **C37receiver** and it is deployed to the relay RIAPS node. **C37receiver** only has one **component** called **C37device** which can communicate with the PCC relay using IEEE C37.118.2 synchrophasor data transfer protocol. The PCC relay constantly measures the voltage magnitude, frequency and phase difference between the main grid and MG. The measurement data along with the relay status are sent to the relay RIAPS node using C37 messages. Upon receiving the C37 message from the relay, the relay RIAPS node will pack the data under the topic **SyncData** and publish it across the RIAPS network. **SyncData** is subscribed by the DG RIAPS node and will be used for the synchronization algorithm.

On each DG, one **actor** called **Synchronizer** is deployed to realize the proposed phase/frequency regulator. The **actor** has two **components**. One is called **ModbusDevice** and used to provide Modbus communication with DG's local controller. The other is called **Regulation** and used to realize the developed distributed algorithm on phase/frequency regulation, as shown in (1). On one hand, the **ModebusDevice** sends out a request to pull out the local measurements (ω_i and $\frac{Q_i}{Q_i^*}$) every time step. On the other hand, voltage phasor mismatch (ω_G, $\Delta\delta_c$ and ΔE_C) are received from the relay RIAPS node. These information are passed to **Regulation** to calculate the updated synchronization control variables (Ω_i, $\widehat{\omega}_i$ and e_i). The updated synchronization control variables are then sent back to the DG's local controller through another Modbus message. At last, each RIAPS node will publish its updated variables for synchronization control (Ω_i, $\widehat{\omega}_i$ and $\frac{Q_i}{Q_i^*}$) while receive the ones from its neighbouring DGs. The updated variables are recorded by **Regulation**.

V. Hardware Implementation and Experimental Results

Validation of the proposed MG synchronization controller is done using a real-time CHIL MG testbed developed in our lab.

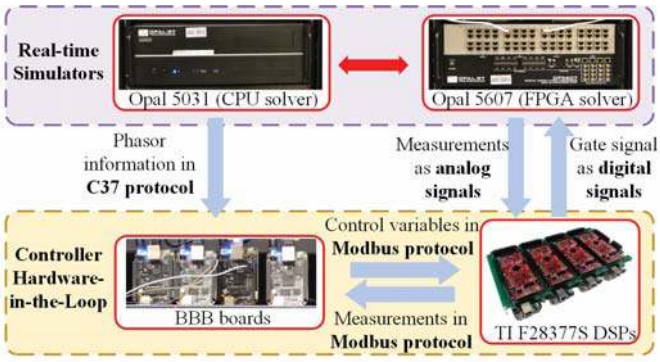

Fig. 3: Real-time controller hardware-in-the-loop MG testbed setup

The presented CHIL testbed aims to provide a comprehensive replication of the operation environment under which the proposed synchronization controller is supposed to serve and the testbed setup is shown in Fig. 3. The presented MG testbed consists of two major parts: 1) Opal-RT real-time simulators are utilized to simulate the MG system operation status under different levels of details. Non-switching components in the MG system, like transformer or relay, are simulated using CPU-based solver under 80 μs simulation time step; while switching-based devices, like converters, are simulated using FPGA-based solver under 500 ns simulation time step. In [18] , it is shown that the fast transient dynamics of power electronics converter can be captured using this testbed. 2) Hardware controllers are integrated with the real-time simulators to accurately replicate the controller response. Beaglebone Black board (BBB) is selected as the hardware controller and each agent (DGs and relay in this case) is assigned with one BBB as the local intelligence. The proposed MG synchronization controller has been fully implemented in the BBBs and the execution and coordination of each BBB is achieved using RIAPS platform. TI F28377S DSPs are used as the primary controller of each DG inverter. Droop control is implemented in each DSP and each DSP is assigned with one BBB that provides secondary level control.

As shown in Fig. 3, the presented MG testbed is integrated using multiple communication channels and forms. The voltage phasor mismatch at PCC is first shared to the relay BBB using IEEE C37 communication protocol and then processed among DG BBBs using RIAPS platform. Data exchange between each DG BBB and its assigned DSP is achieved using Modbus communication protocol. Each DG BBB shall update

TABLE I: MG testbed parameters

DG (kW/kVAR)		Critical Load (kW/kVAR)	
P^*=100	Q^*=100	P_L=50	Q_L=24
Control Gain Design			
m^{-1}=100000	n^{-1}=10000	$k_f = 0.033$	$k_P = 0.4$
$r = 0.01$	k_ω=0.1	k_Q=0.001	β=0.03125

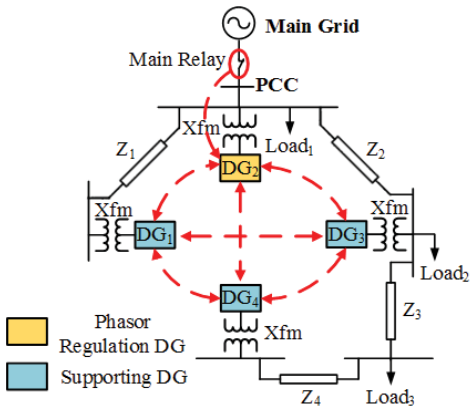

Fig. 4: Simulated MG system topology

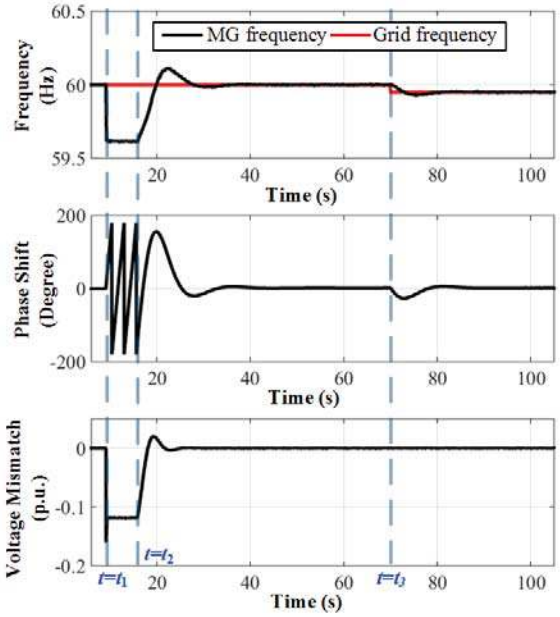

Fig. 5: Recorded system operation states experimental results

its control variables using both the local measurements from its assigned DSP and the information shared by its neighbour DG BBB(s). Operation status of each DG inverter is directly controlled by the digital gate signals from its assigned DSP, which depend on the control variables from BBB and the droop control using local measurements as analog signals.

The MG topology under study is presented in Fig. 4. Four DGs (DG_1, DG_2, DG_3 and DG_4) and three critical loads ($S_L = S_{L1} = S_{L3} = 0.5S_{L2}$) are presented and DG_2 is selected as the phasor regulation DG. Communication links among relay and DGs are presented in red dashed lines. Detailed testbed parameters are provided in Table I and the control gains are designed based on the stability analysis derived in previous section.

The dynamic performance of the proposed MG synchronization controller with main grid frequency variation is simulated and the recorded system operation states measured at PCC are presented in Fig. 5. As shown in Fig. 5, the MG initially operates under grid connected mode and the main relay opens at $t = t_1$. The islanded MG is first stabilized by droop control which results in steady state deviations on system frequency and voltage. The proposed MG synchronization controller is initiated at $t = t_2$, it can be observed that as the system converges, the islanded MG and the main grid operate under the same frequency ($\omega_G = 60$ Hz) and voltage mismatch measured at PCC on phase and voltage magnitude are eliminated. A step change on the main grid frequency ($|\Delta\omega_G| = 0.05$ Hz) is introduced at $t = t_3$. It can be observed that as the system converges, the proposed controller is able to have the islanded MG operates synchronously with the main grid even if the main grid is not operated under rated frequency. Fig. 6 shows the zoomed in system response during main grid frequency deviation. It can be observed that as the main grid frequency changes, the islanded MG frequency is able to accurately follow the one of the main grid. New phase mismatch is introduced due to the instant frequency mismatch between the main grid and islanded MG but such mismatch is eliminated eventually. It is noteworthy that no deviations on voltage mismatch is observed in Fig. 6, which validates the assumptions made in system stability analysis that system voltage/reactive power variation and frequency/active power variation are decoupled. Additionally, active and reactive power sharing among all the DGs are always maintained in steady state, as shown in Fig. 7.

VI. Conclusions

A distributed MG synchronization operation algorithm is proposed in this paper. The proposed algorithm is able to keep the voltage phasor at the MG side of PCC synchronized with the one on the main grid side. System frequency, phase and voltage magnitude mismatch are regulated explicitly at the same time, and the system total load are proprotionally shared by all the DGs. Exponential stability of the proposed controller is derived and its dynamic performance is validated using a CHIL MG testbed. The proposed controller is fully implemented in hardware controllers using the RIAPS platform developed by our team. The proposed MG synchronization controller is proved to be effect by the experimental results.

Acknowledgment

This work was funded in part by the Advanced Research Projects Agency-Energy (ARPA-E), U.S. Department of Energy, under Award Number DE-AR0000666. The views and opinions of authors expressed herein do not necessarily state or reflect those of the US Government or any agency thereof.

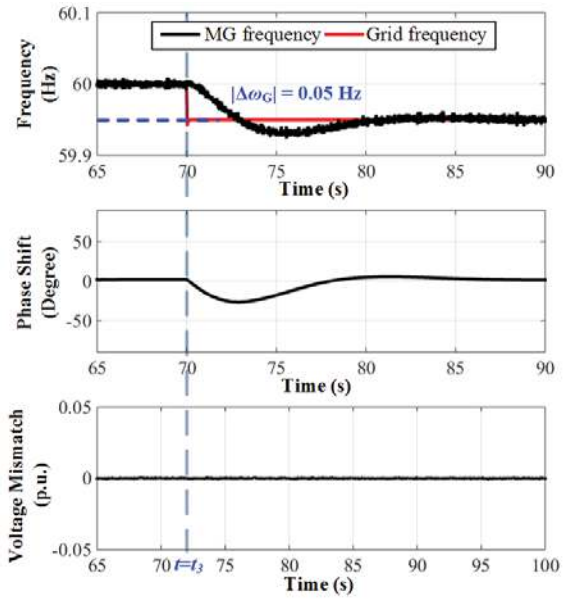

Fig. 6: Recorded system operation states experimental results (zoom-in)

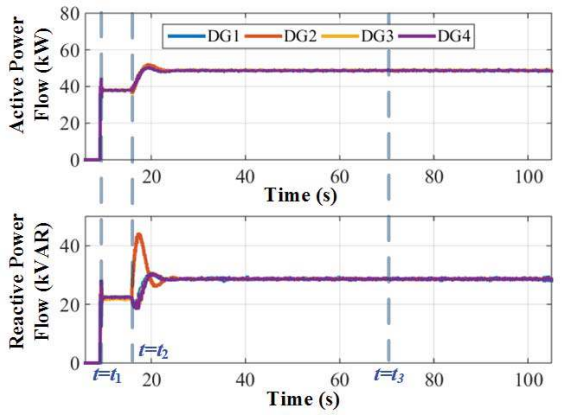

Fig. 7: Recorded DG power outputs experimental results

REFERENCES

[1] F. Tang, J. M. Guerrero, J. C. Vasquez, D. Wu, and L. Meng, "Distributed active synchronization strategy for microgrid seamless reconnection to the grid under unbalance and harmonic distortion," *IEEE Transactions on Smart Grid*, vol. 6, no. 6, pp. 2757–2769, 2015.

[2] "SGIP OpenFMB microgrid reconnection use case," https://members.sgip.org/higherlogic/ws/public/download/9413/SGIP, 11 2016.

[3] S. S. Thale and V. Agarwal, "Controller area network assisted grid synchronization of a microgrid with renewable energy sources and storage," *IEEE Transactions on Smart Grid*, vol. 7, no. 3, pp. 1442–1452, 2016.

[4] G. Chen and E. Feng, "Distributed secondary control and optimal power sharing in microgrids," *IEEE/CAA Journal of Automatica Sinica*, vol. 2, no. 3, pp. 304–312, 2015.

[5] T. M. L. Assis and G. N. Taranto, "Automatic reconnection from intentional islanding based on remote sensing of voltage and frequency signals," *IEEE Transactions on Smart Grid*, vol. 3, no. 4, pp. 1877–1884, 2012.

[6] Q. Shafiee, J. M. Guerrero, and J. C. Vasquez, "Distributed secondary control for islanded microgridsa novel approach," *IEEE Transactions on power electronics*, vol. 29, no. 2, pp. 1018–1031, 2014.

[7] D. Shi, X. Chen, Z. Wang, X. Zhang, Z. Yu, X. Wang, and D. Bian, "A distributed cooperative control framework for synchronized reconnection of a multi-bus microgrid," *IEEE Transactions on Smart Grid*, 2017.

[8] Y. Sun, C. Zhong, X. Hou, J. Yang, H. Han, and J. M. Guerrero, "Distributed cooperative synchronization strategy for multi-bus microgrids," *International Journal of Electrical Power & Energy Systems*, vol. 86, pp. 18–28, 2017.

[9] C. Papadimitriou, V. Kleftakis, and N. Hatziargyriou, "Control strategy for seamless transition from islanded to interconnected operation mode of microgrids," *Journal of Modern Power Systems and Clean Energy*, vol. 5, no. 2, pp. 169–176, 2017.

[10] J. M. Guerrero, M. Chandorkar, T.-L. Lee, and P. C. Loh, "Advanced control architectures for intelligent microgridspart i: Decentralized and hierarchical control," *IEEE Transactions on Industrial Electronics*, vol. 60, no. 4, pp. 1254–1262, 2013.

[11] J. He and Y. W. Li, "Analysis, design, and implementation of virtual impedance for power electronics interfaced distributed generation," *IEEE Transactions on Industry Applications*, vol. 47, no. 6, pp. 2525–2538, 2011.

[12] B. Liu, W. Lu, and T. Chen, "Pinning consensus in networks of multiagents via a single impulsive controller," *IEEE transactions on neural networks and learning systems*, vol. 24, no. 7, pp. 1141–1149, 2013.

[13] J. W. Simpson-Porco, Q. Shafiee, F. Dörfler, J. C. Vasquez, J. M. Guerrero, and F. Bullo, "Secondary frequency and voltage control of islanded microgrids via distributed averaging," *IEEE Transactions on Industrial Electronics*, vol. 62, no. 11, pp. 7025–7038, 2015.

[14] J. W. Simpson-Porco, F. Dörfler, and F. Bullo, "Synchronization and power sharing for droop-controlled inverters in islanded microgrids," *Automatica*, vol. 49, no. 9, pp. 2603–2611, 2013.

[15] J. M. Guerrero, J. C. Vasquez, J. Matas, L. G. De Vicuña, and M. Castilla, "Hierarchical control of droop-controlled ac and dc microgridsa general approach toward standardization," *IEEE Transactions on industrial electronics*, vol. 58, no. 1, pp. 158–172, 2011.

[16] Y. Du, H. Tu, S. Lukic, D. Lubkeman, A. Dubey, and G. Karsai, "Implementation of a distributed microgrid controller on the resilient information architecture platform for smart systems (riaps)," in *2017 North American Power Symposium (NAPS)*, Sept 2017, pp. 1–6.

[17] A. Dubey, G. Karsai, P. Volgyesi, M. Metelko, I. Madari, H. Tu, Y. Du, and S. Lukic, "Device access abstractions for resilient information architecture platform for smart grid," *IEEE Embedded Systems Letters*, pp. 1–1, 2018.

[18] H. Yu, H. Tu, and S. Lukic, "A passivity-based decentralized control strategy for current-controlled inverters in ac microgrids," in *2018 IEEE Applied Power Electronics Conference and Exposition (APEC)*, March 2018, pp. 1399–1406.